

Electronic and Magnetic Structures of Chain Structured Iron Selenide Compounds

Wei Li,¹ Chandan Setty,² X. H. Chen,³ and Jiangping Hu^{4,2,*}

¹*Department of Physics, Fudan University, Shanghai 200433, China*

²*Department of Physics, Purdue University, West Lafayette, Indiana 47907, USA*

³*Hefei National Laboratory for Physical Science at Microscale and Department of Physics, University of Science and Technology of China, Hefei, Anhui 230026, China*

⁴*Beijing National Laboratory for Condensed Matter Physics, and Institute of Physics, Chinese Academy of Sciences, Beijing 100190, China*

(Dated: March 9, 2021)

Electronic and magnetic structures of iron selenide compounds $\text{Ce}_2\text{O}_2\text{FeSe}_2$ (2212*) and BaFe_2Se_3 (123*) are studied by the first-principles calculations. We find that while all these compounds are composed of one-dimensional (1D) Fe chain (or ladder) structures, their electronic structures are not close to be quasi-1D. The magnetic exchange couplings between two nearest-neighbor (NN) chains in 2212* and between two NN two-leg-ladders in 123* are both antiferromagnetic (AFM), which is consistent with the presence of significant third NN AFM coupling, a common feature shared in other iron-chalcogenides, FeTe (11*) and $\text{K}_y\text{Fe}_{2-x}\text{Se}_2$ (122*). In magnetic ground states, each Fe chain of 2212* is ferromagnetic and each two-leg ladder of 123* form a block-AFM structure. We suggest that all magnetic structures in iron-selenide compounds can be unified into an extended J_1 - J_2 - J_3 model. Spin-wave excitations of the model are calculated and can be tested by future experiments on these two systems.

PACS numbers: 74.25.Jb, 74.70.-b, 74.25.Ha, 71.20.-b

I. INTRODUCTION

The newly discovered 122*, $A_y\text{Fe}_{2-x}\text{Se}_2$, iron-chalcogenide superconductors¹⁻⁵ have attracted enormously interests. Like iron-pnictide high temperature superconductors, the FeSe-based superconductors have the same robust tetrahedral layers structure. However, there are a number of distinct intriguing physical properties which are noticeably absent in iron-pnictide materials. Such as antiferromagnetically (AFM) ordered insulating phases^{5,6}, extremely high Néel transition temperatures^{7,8}, and the presence of intrinsic Fe vacancies and ordering⁹⁻¹². In addition, the Fermi surface (FS) topologies of superconducting compounds are very different from previously known superconducting Fe-pnictides. Both band structures calculations¹³⁻¹⁶ and angle resolved photoemission spectroscopy studies^{17,18} indicated that only the electron pockets are present in the superconducting compounds, while the hole pockets around Γ point observed in iron-pnictide counterparts sink below the Fermi level, indicating that the inter-pocket scattering between the hole and electron pockets is not an essential ingredient for superconductivity.

Following the discovery of the 122* iron-chalcogenide, two new materials, $\text{Ce}_2\text{O}_2\text{FeSe}_2$ (2212*)¹⁹ and BaFe_2Se_3 (123*)²⁰⁻²³, have been synthesized. In the 2212*, each Fe-layer is composed of coupled one-dimensional (1D) Fe-chains and in the 123*, it is structured by coupled two-leg ladders. An analogy of these materials can be made to those in cuprates, such as a spin-ladder system $\text{Sr}_{14-x}\text{Ca}_x\text{Cu}_{24}\text{O}_{41}$ ^{24,25} ($x=11.5-15.5$) and a double chain system $\text{Pr}_2\text{Ba}_4\text{Cu}_7\text{O}_{15-\delta}$ ²⁶. 123*²⁰⁻²³, which has been investigated intensively. It was also reported that the 123* may be superconducting²⁰.

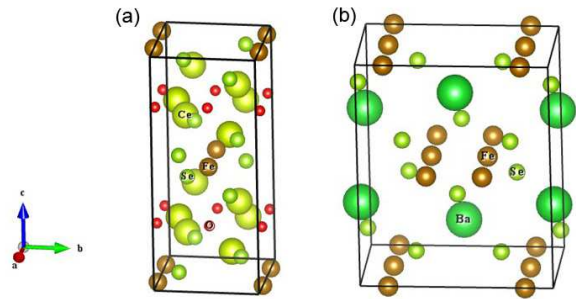


FIG. 1: (Color online) Calculated crystal structures of the iron selenide compounds: (a) 2212*, which consists of one chain of FeSe_4 tetrahedra structure, and (b) 123*, which consists of two-leg-ladders of edge-sharing FeSe_4 tetrahedra structure, respectively.

In this paper, we present the theoretical study of the electronic band structures and magnetic orders in these iron selenide systems featured with low-dimensional iron structures. We investigate two materials including 2212* and 123* and show that while all these compounds are composed of 1D Fe chain structures, their electronic structures are not close to be quasi-1D. Their FS still exhibit two dimensional or even three dimensional topologies. We calculate their magnetic ordered ground states. In 2212*, the magnetic order ground state is a collinear-AFM (CAF), similar to iron-pnictides. In 123*, the magnetic structure is a block-AFM (BAF), similar to KFe_2Se_2 ²⁷. The magnetic exchange couplings between two nearest neighbor (NN) chains in 2212* and between two NN two-leg-ladders in 123* are both AFM, which is consistent with the presence of significant third NN AFM

TABLE I: Structural parameters, density of states at the Fermi level $N(E_F)$ (in the $(\text{eV})^{-1}$ units per Fe atom) and the calculated specific heat coefficient $\gamma_0[mJ/(K^2mol)]$, and Pauli susceptibility $\chi_0(10^{-9}m^3/mol)$ for iron selenide compounds in NM state. The lattice parameters and the internal coordinates are all optimized within energy minimization.

	$a(\text{\AA})$	$b(\text{\AA})$	$c(\text{\AA})$	$N(E_F)$	γ_0	χ_0
2212*	5.5508	5.6794	16.2566	6.7293	31.7196	5.4546
123*	5.3821	9.1123	11.2096	0.7650	3.6060	0.6201

coupling, J_3 , in FeTe (11*) and 122*. This result suggests that all magnetic structures in iron selenide compounds can be unified into an extended J_1 - J_2 - J_3 model. We also calculate spin-wave excitations of the model which can be tested in future experiments on these two systems.

II. THEORIES AND RESULTS

A. First-Principles Calculations

We perform the first-principles calculations on the iron selenide compounds: 2212*, which has 1D chains of edge-shared FeSe_4 tetrahedra structure and 123*, which consists double chains (two-legged ladders) of edge-shared FeSe_4 tetrahedra structure. The crystal structures are shown in Fig. 1. In our calculations the projected augmented wave method²⁸ as implemented in the VASP code²⁹, and the Perdew-Burke-Ernzerhof exchange correlation potential³⁰ was used. All atomic positions and the lattice constants are allowed to relax simultaneously to minimize the energy only for nonmagnetic (NM) state. The experimental crystal structures^{19,21} are used for calculating magnetic states. A 500eV cutoff in the plane wave expansion ensures the calculations converge to 10^{-5} eV, and all atomic positions and the lattice constants were optimized until the largest force on any atom was $0.005\text{eV}/\text{\AA}$. To properly describe the strong electron correlation in the $4f$ rare earth element Ce, the LDA plus on-site repulsion U method (LDA+ U) was employed with the effective U value ($U_{eff} = U - J$) of 12.0eV for the compound 2212*, where the U_{eff} value has been reported in the previous work³¹ of CeOFeAs . The results are also checked for consistency with varying U_{eff} values. We do not apply U_{eff} to the itinerant Fe- $3d$ states.

First, we focus on the electronic structures of the iron selenide compounds and their dependence on the structural factors. For this purpose, full structural optimization of the these compounds were performed both over the lattice parameters and the atomic positions including the internal coordinate z of Se atom by the energy minimization. All these results (not included the internal coordinate) are summarized in the Table I. Actually, both iron selenide compounds of the lattice parameters optimized in our NM calculations are found smaller by about 2% than the ones in experimental values¹⁹⁻²². In

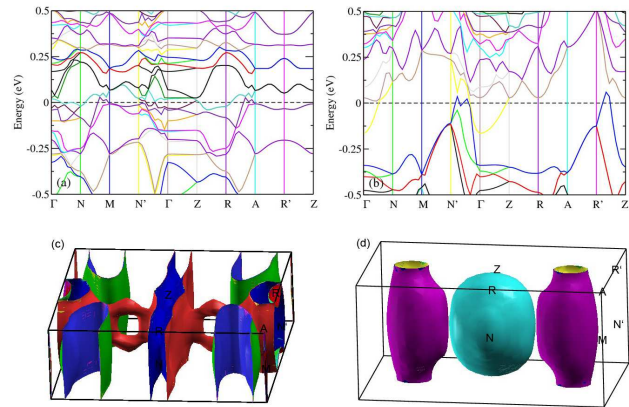


FIG. 2: (Color online) Electronic structures of the iron selenide compounds in the NM state: The band structure of 2212* (a), 123* (b), and the corresponding FS (c) and (d), respectively. The Fermi energy is set to zero.

addition, the density of states $N(E_F)$ at the Fermi energy are also calculated, and the corresponding electronic specific heat coefficient γ_0 and Pauli susceptibility χ_0 are all listed in Table I.

Figure 2 shows the NM state band structure and FS of both iron selenide compounds. As we can see that there are three bands crossing the Fermi level for both iron selenide compounds. Although both iron selenide compounds are composed of 1D Fe chain (ladder) structures and exhibit quasi-1D characters, their FSs still exhibit two-dimensional or even three dimensional complex topologies. Their NM state electronic structures are very distinct from that of the iron selenide superconductor KFe_2Se_2 ¹⁴⁻¹⁷. Therefore, if superconductivity exists in these compounds, it provides a new playground to test theoretical mechanisms.

Because the NM state is strongly unstable against moment formation, we turn to study the magnetic structures in both iron selenide compounds. The six different possible magnetic configurations, as shown in Fig. 3 [ferromagnetic (FM) state has not been included] are all calculated. In Table II, we list the energies of different magnetic states. For 2212*, it is shown that the CAF is the lowest energy state. In the CAF state of 2212*, spins are FM for each Fe-chains and are AFM between two NN chains. The calculated magnetic moment around each Fe ion is found to be about $3.12\mu_B$, which is well consistency with experimental results $3.33\mu_B$ at low temperature 12K¹⁹. Furthermore, the calculated band structure of CAF state is shown that 2212* is a semiconductor with an energy band gap of around 0.64eV, as shown in Fig. 4(a), which is also well consistency with reported experimental results¹⁹. For 123*, the BAF state is the lowest energy state. In the BAF state of 123*, for each two-leg ladder, four spins group together become a superunit. Spins between two NN units are AFM. The coupling between two NN two-leg ladders is also AFM. The moment

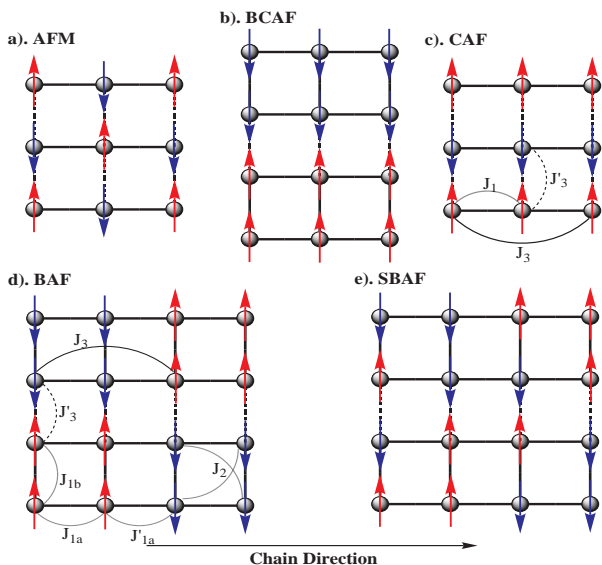


FIG. 3: (Color online) Schematic top view of five possible magnetic orders in the Fe-Fe square layer of the iron selenide compounds: (a) AFM Néel order in which the nearest neighboring Fe moments are AFM ordered; (b) Bicollinear-AFM (BCAF) order (the chain direction is changed into vertical direction for 2212*); (c) CAF order in which the Fe moments are FM ordered along the chain direction and AFM ordered across the chains direction; (d) BAF consisting of FM Fe_4 plaquettes tiled AFM along the chain direction; (e) Staggered-BAF (SBAF) configuration with FM diagonal double stripes that are also tiled AFM.

around each Fe is about $2.85\mu_B$ for 123*, and the electronic band structure calculated shows a semiconductor with an energy band gap $E_g=0.24\text{eV}$, as shown in Fig. 4(b). The very small energy difference between FM state and CAF state is indicative of weak AFM coupling between different chains, and the energy difference between AFM state and CAF state is indicative of strong FM coupling along the chain direction in 2212*. Similarly, in 123* system, the small energy difference between FM state and BCAF state is also indicative of weak AFM coupling between different ladders, and the energy difference between BAF state and BCAF state indicative of four Fe atom plackets along the ladders.

Nevertheless, these results are consistent with magnetic exchange couplings obtained in other iron-chalcogenides FeTe and $\text{K}_{0.8}\text{Fe}_{1.6}\text{Se}_2$, where an FM NN coupling J_1 , an AFM next nearest neighbor (NNN) coupling J_2 , and an third NN AFM J_3 are necessary in describing magnetic orders. As we will show in next subsection, the magnetic orders of both materials can be obtained within models with the similar exchange coupling parameters. The AFM couplings between two NN chains in the 2212* and between two NN two-leg ladders in the 123* are exactly the third NN AF coupling, J_3 . The BAF order within each two-leg ladder can also be naturally understood from these couplings. Therefore, overall, the magnetism of all iron-chalcogenides can be

TABLE II: Energetic and magnetic properties of the 2212* and 123*. Results in the magnetic states configurations, as shown in Fig. 3 using experimental crystal structures^{19,21}. ΔE is the total energy difference per iron atom in reference to the FM state, and m_{Fe} is the local magnetic moment on Fe.

	2212*	123*
	$\Delta E(\text{eV})/m_{\text{Fe}}(\mu_B)$	$\Delta E(\text{eV})/m_{\text{Fe}}(\mu_B)$
FM	0/3.13	0/2.58
AFM	0.2184/3.11	-0.1131/2.38
CAF	-0.0118 /3.12	-0.1560/2.77
BCAF	0.0944/3.13	-0.0139/2.55
BAF	—	-0.1615 /2.85
SBAF	—	-0.1514/2.74

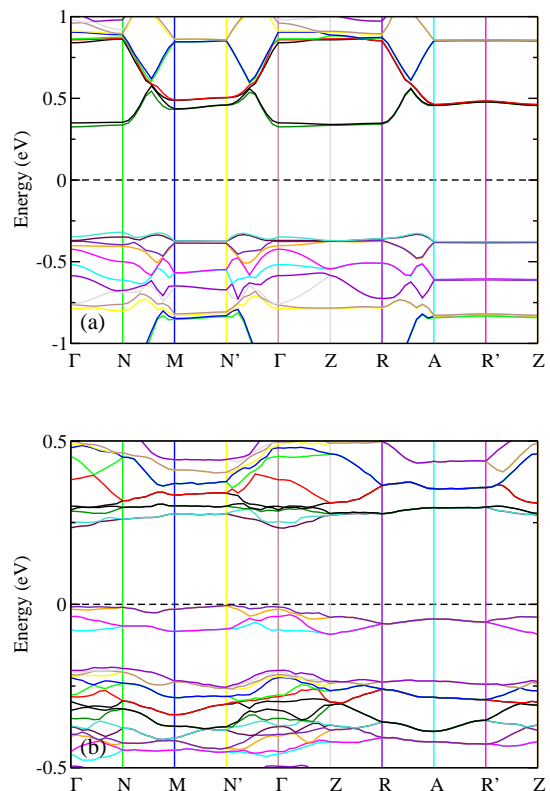


FIG. 4: (Color online) (a) Electronic band structure of the CAF state in 2212* with an energy band gap $E_g = 0.64\text{eV}$; (b) Electronic band structure of the BAF state in 123* with an energy band gap $E_g=0.24\text{eV}$. The Fermi energy is set to zero.

unified into an effective model that includes local magnetic exchange couplings as suggested in 32 and 33. The values of exchange couplings can not be accurately determined since the result depends on the selection of the magnetic configurations²⁷.

B. Magnetic Model for $\text{Ce}_2\text{O}_2\text{FeSe}_2$

Following above results and effective models derived for other iron-chalcogenides, we construct the following model to describe this material

$$\hat{H} = J_1 \sum_{\langle i,j \rangle} \vec{S}_i \cdot \vec{S}_j + J_3 \sum_{\langle\langle i,j \rangle\rangle} \vec{S}_i \cdot \vec{S}_j + J'_3 \sum_{\langle i,j \rangle} \vec{S}_i \cdot \vec{S}_j, \quad (1)$$

where J_1 and J_3 are the NN and next NN intrachain magnetic exchange couplings and J'_3 is the NN interchain magnetic exchange coupling, as shown in Fig. 3(c).

The classical ground state of the Hamiltonian can be obtained exactly. In general, the classical energy is given as (for simplicity, we take $S = 1$)

$$E_c = 2J_1 \cos Q_x + 4J_3 (\cos^2 Q_x - 1/2) + 2J'_3 \cos Q_y,$$

where (Q_x, Q_y) are the magnetic order wavevectors which can be viewed as the relative polarization angles between two NN intrachain spins and interchain spins respectively. The CAF phase is obtained when $J_3 < |J_1|/4$ and $J'_3 > 0$.

In this state, we perform a linear spin wave analysis for this material in the classical limit. To do this we use the usual linearized Holstein-Primakoff transformation from spin operators to magnon operators which read as

$$S_i^x = \sqrt{\frac{S}{2}}(b_i + b_i^\dagger); S_i^y = -i\sqrt{\frac{S}{2}}(b_i - b_i^\dagger); S_i^z = S - b_i^\dagger b_i$$

where i runs over all the lattice sites. Performing a fourier transform, the spin wave excitations of the model is given by

$$\hat{H} = H_0 + \sum_k \Psi_k^\dagger \begin{pmatrix} a_k & b_k \\ b_k & a_k \end{pmatrix} \Psi_k, \quad (2)$$

where, $H_0 = 2NJ_1 + 2NJ_2 - 2NJ_3$ is the ground state energy and $\Psi_k^\dagger = (b_k^\dagger, b_{-k})$, where

$$\begin{aligned} a_k &= J_1(\cos k_x - 1) + J_3(\cos 2k_x - 1) + J'_3 \\ b_k &= J'_3 \cos k_y \end{aligned}$$

Using the Bogliubov transformation, the linear spin-wave approximation, Eq. (2) can be diagonalized and shown in Fig. 5. It is interesting to see the effect of J_3 on the spin wave excitations. For J_3 being AFM and close to $0.25J_1$, the spin wave dispersion along chain direction (k_x, π) becomes quadratic at $k_x = 0$. Otherwise, the dispersion is linear.

C. Magnetic model for BaFe_2Se_3

For the 123^* system, we can begin with the following general Hamiltonian,

$$\begin{aligned} \hat{H} &= J_{1b} \sum_{\langle i,j \rangle} \vec{S}_i \cdot \vec{S}_j + J_{1a} \sum_{\langle i,j \rangle} \vec{S}_i \cdot \vec{S}_j + J'_{1a} \sum_{\langle i,j \rangle} \vec{S}_i \cdot \vec{S}_j \\ &+ J_2 \sum_{\langle\langle i,j \rangle\rangle} \vec{S}_i \cdot \vec{S}_j + J_3 \sum_{\langle\langle\langle i,j \rangle\rangle\rangle} \vec{S}_i \cdot \vec{S}_j + J'_3 \sum_{\langle i,j \rangle} \vec{S}_i \cdot \vec{S}_j, \end{aligned}$$

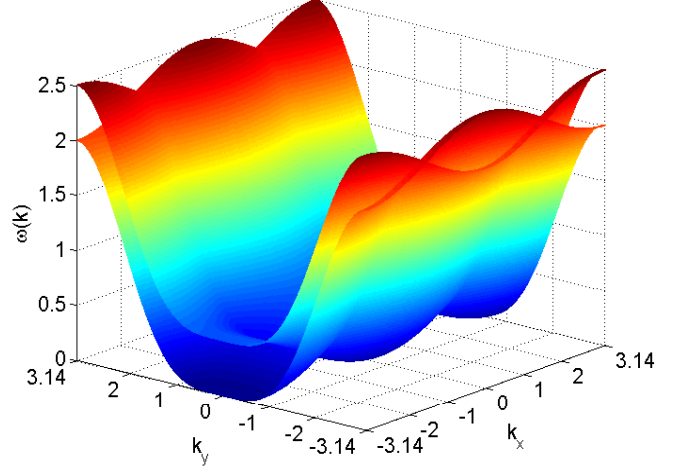


FIG. 5: (Color online) The spin wave dispersion relation as a function of k_x - k_y in the commensurate phase $(0, \pi)$ CAF state for 2212^* . Parameters chosen are $(J_1, J_3, J'_3) = (-1, 0.25, 0.25)$.

where J_{1b} along with J_{1a}, J'_{1a} and J_3 denote the intraladder vertical and horizontal NN and the third NN couplings, J_2 is the intraladder diagonal coupling and J'_3 is the interladder interaction as shown in Fig. 3(c). These coupling parameters reflect the symmetry breaking of the BAF state.

We can treat the above model classically to obtain the exact ground state and phase diagram. We define the relative polarization angles (Q_x, Q'_x, Q_y, Q'_y) along the different directions, with the primed variables going with the respective primed couplings. We can then write off the classical ground state energy as (for simplicity, we also take $S = 1$)

$$\begin{aligned} E_c &= 2J'_3 \cos Q'_y + 2J_{1b} \cos Q_y + 2J_{1a} \cos Q_x \\ &+ 2J'_{1a} \cos Q'_x + 2J_2 \cos Q_y \cos Q'_x \\ &+ 2J_2 \cos Q_y \cos Q_x + 4J_3 \cos(Q_x + Q'_x) \end{aligned}$$

We can then obtain the ground states by simply minimizing the classical energy. With the BAF state being the ground state, we have $(Q_x, Q'_x, Q_y, Q'_y) = (0, \pi, 0, \pi)$. Following the exchange coupling values measured for FeTe^{34} and $\text{K}_{0.8}\text{Fe}_{1.6}\text{Se}_2^{35}$, we expect that $J_{1a} \sim J_{1b} < 0$, $J_3 > 0$, $J'_3 > 0$, $J_2 > 0$, and $J'_{1a} > 0$. The strength of the couplings satisfies, $|J_{1a}| > J_2 > J_3, J'_3, J'_{1a}$, which stabilizes the BAF phase.

In the BAF state, we can obtain the spin wave excitations as done previously, which is given by

$$H = H_0 + \frac{1}{2} \sum_k \Psi_k^\dagger \begin{pmatrix} A_k & B_k \\ B_k & A_k \end{pmatrix} \Psi_k, \quad (3)$$

where $H_0 = NJ_{1a} + NJ_{1b} - NJ'_{1a} - 2NJ_3 - NJ'_3$ is the ground state energy and $\Psi_k^\dagger =$

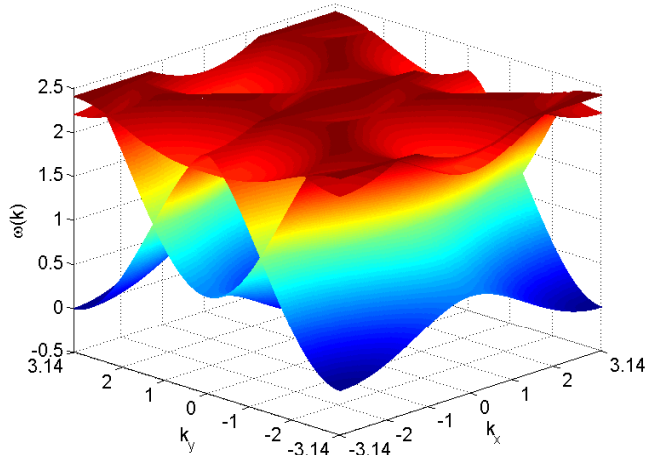


FIG. 6: (Color online) The spin wave dispersion relation of the lowest three branches (the other one is too high to be drawn in the same plot) as a function of k_x - k_y in the BAF state for 123^* . The chosen parameters are fixed as $(J_{1a}, J'_{1a}, J_{1b}, J_2, J_3, J'_3) = (-1, 0.1, -1, 0.5, 0.3, 0.3)$.

$(b_{1k}^\dagger, b_{2k}^\dagger, b_{3k}^\dagger, b_{4k}^\dagger, b_{1,-k}, b_{2,-k}, b_{3,-k}, b_{4,-k})$. A_k and B_k are four-by-four matrices, defined by:

$$A_k = \begin{pmatrix} E_0 & J_{1a} & J_2 & J_{1b} \\ \cdot & E_0 & J_{1b} & J_2 \\ \cdot & \cdot & E_0 & J_{1a} \\ \cdot & \cdot & \cdot & E_0 \end{pmatrix} \quad (4a)$$

$$B_k = \begin{pmatrix} E'_0 & J'_{1a}e^{-ik_x} & J_2e^{-ik_x} & J'_3e^{-ik_y} \\ \cdot & E'_0 & J'_3e^{-ik_y} & J_2e^{ik_x} \\ \cdot & \cdot & E'_0 & J'_{1a}e^{ik_x} \\ \cdot & \cdot & \cdot & E'_0 \end{pmatrix} \quad (4b)$$

where $E_0 = -J_{1a} - J_{1b} + J'_{1a} + J'_3 + 2J_3$ and $E'_0 =$

$2J_3 \cos k_x$. The lower triangle elements are suppressed because both matrices are hermitian.

By diagonalizing this Hamiltonian Eq. 3 for each k in the Bosonic metric, we obtain the spin wave dispersion shown in Fig. 6 by taking $J_{1a} = J_{1b} = -1, J_2 = 0.5, J_3 = J'_3 = 0.3, J'_{1a} = 0.1$. The spin wave has four branches which is very similar to the BAF state discussed for KFe_2Se_2 ²⁷.

III. CONCLUSION

In this paper, we have performed the first-principles calculations for the electronic band structures and magnetic orders in these iron selenide systems featured with quasi-1D Fe chain (ladder) structures including 2212^* and 123^* . However, the calculated FS topologies still exhibit two dimensional or even three dimensional features. For 2212^* , we find that the ground state is a CAF ordered semiconductor with an energy gap of 0.64eV, in agreement with the experimental measurements. For 123^* , the calculated results show that the ground state is a BAF ordered semiconductor with an energy gap of 0.24eV. These results suggest that that all magnetic structures in iron selenide compounds can be unified into an extended J_1 - J_2 - J_3 model. We also calculate spin-wave excitations of the model which can be tested in future experiments on these two systems.

Acknowledgement

We thank H. Ding, D. L. Feng, P. C. Dai, N. L. Wang, H. H. Wen, C. Fang and Uday Kiranfor for useful discussion. W.L. gratefully acknowledges the financial support by Research Fund of Fudan University for the Excellent Ph.D. Candidates. The work was supported by the 973 Projects of China (2012CB821400) and NSFC-11190024.

* Electronic address: jphu@iphy.ac.cn

¹ J. Guo, S. Jin, G. Wang, S. Wang, K. Zhu, T. Zhou, M. He, and X. Chen, Phys. Rev. B **82**, 180520(R) (2010).

² H. Lei, and C. Petrovic, Phys. Rev. B **83**, 180503(R) (2011).

³ A Krzton-Maziopa, Z Shermadini, E Pomjakushina, V Pomjakushin, M Bendele, A Amato, R Khasanov, H Luetkens, and K Conder, J. Phys.: Condens. Matter **23**, 052203 (2011).

⁴ R. H. Liu, X. G. Luo, M. Zhang, A. F. Wang, J. J. Ying, X. F. Wang, Y. J. Yan, Z. J. Xiang, P. Cheng, G. J. Ye, Z. Y. Li, and X. H. Chen, Europhys. Lett. **94**, 27008 (2011).

⁵ M. Fang, H. Wang, C. Dong, Z. Li, C. Feng, J. Chen, and H. Q. Yuan, Europhys. Lett. **94**, 27009 (2011).

⁶ Z. G. Chen, R. H. Yuan, T. Dong, G. Xu, Y. G. Shi, P.

Zheng, J. L. Luo, J. G. Guo, X. L. Chen, and N. L. Wang, Phys. Rev. B **83**, 220507(R) (2011).

⁷ W. Bao, Q. Huang, G. F. Chen, M. A. Green, D. M. Wang, J. B. He, X. Q. Wang, and Y. Qiu, Chinese Phys. Lett. **28**, 086104 (2011).

⁸ V. Yu. Pomjakushin, D. V. Sheptyakov, E. V. Pomjakushina, A. Krzton-Maziopa, K. Conder, D. Chernyshov, V. Svitlyk, and Z. Shermadini, Phys. Rev. B **83**, 144410 (2011).

⁹ Z. Wang, Y. J. Song, H. L. Shi, Z. W. Wang, Z. Chen, H. F. Tian, G. F. Chen, J. G. Guo, H. X. Yang, and J. Q. Li, Phys. Rev. B **83**, 140505(R) (2011).

¹⁰ P. Zavalij, W. Bao, X. F. Wang, J. J. Ying, X. H. Chen, D. M. Wang, J. B. He, X. Q. Wang, G. F. Chen, P.-Y. Hsieh, Q. Huang, and M. A. Green, Phys. Rev. B **83**, 132509

- (2011).
- ¹¹ X.-W. Yan, M. Gao, Z.-Y. Lu, and Tao Xiang, *Phys. Rev. B* **83**, 233205 (2011).
 - ¹² C. Cao and J. Dai, *Phys. Rev. Lett.* **107**, 056401 (2011).
 - ¹³ I. A. Nebrasov and M. V. Sadovskii, *JETP Lett.* **93**, 166 (2011).
 - ¹⁴ I.R. Shein and A.L. Ivanovskii, arXiv:1012.5164 (2010).
 - ¹⁵ X.-W. Yan, M. Gao, Z.-Y. Lu, and T. Xiang, *Phys. Rev. B* **84**, 054502 (2011).
 - ¹⁶ C. Cao and J. Dai, *Chinese Physics Letter*, **28**, 057402 (2011).
 - ¹⁷ Y. Zhang, L. X. Yang, M. Xu, Z. R. Ye, F. Chen, C. He, J. Jiang, B. P. Xie, J. J. Ying, X. F. Wang, X. H. Chen, J. P. Hu, and D. L. Feng, *Nature Materials* **10**, 273 (2011).
 - ¹⁸ T. Qian, X.-P. Wang, W.-C. Jin, P. Zhang, P. Richard, G. Xu, X. Dai, Z. Fang, J.-G. Guo, X.-L. Chen, and H. Ding, *Phys. Rev. Lett.* **106**, 187001 (2011).
 - ¹⁹ E. E. McCabe, D. G. Free and J. S. O. Evans, *Chem. Commun.*, **47**, 1261 (2011).
 - ²⁰ A. Krzton-Maziopa, E. Pomjakushina, V. Pomjakushin, D. Sheptyakov, D. Chernyshov, V. Svitlyk, K. Conder, arXiv:1108.1670 (2011).
 - ²¹ J. M. Caron, J. R. Neilson, D. C. Miller, A. Llobet, and T. M. McQueen, *Phys. Rev. B* **84**, 180409(R) (2011).
 - ²² B. Saporov, S. Calder, B. Sipos, H. Cao, S. Chi, D. J. Singh, A. D. Christianson, M. D. Lumsden, and A. S. Sefat, *Phys. Rev. B* **84**, 245132 (2011).
 - ²³ J.M. Caron, J.R. Neilson, D.C. Miller, K. Arpino, A. Llobet, T. M. McQueen, arXiv:1202.3676 (2012).
 - ²⁴ E. M. McCarron III, M. A. Subramanian, J. C. Calabrese, and R. L. Harlow, *Mater. Res. Bull.* **23**, 1355 (1988).
 - ²⁵ T. Siegrist, L. F. Schneemeyer, S. A. Sunshine, J. V. Waszczak, and R. S. Roth, *Mater. Res. Bull.* **23**, 1429 (1988).
 - ²⁶ T. Nakano, K. Kuroki, S. Onari, *Physica B: Condensed Matter* **403**, 1159 (2008).
 - ²⁷ W. Li, S. Dong, C. Fang, and J. Hu, arXiv:1110.0372 (2011).
 - ²⁸ P. E. Blöchl, *Phys. Rev. B* **50**, 17953 (1994).
 - ²⁹ G. Kresse and J. Furthmuller, *Phys. Rev. B* **54**, 11169 (1996).
 - ³⁰ J. P. Perdew, K. Burke, and M. Ernzerhof, *Phys. Rev. Lett.* **77**, 3865 (1996).
 - ³¹ L. Pourovskii, V. Vildosola, S. Biermann, A. Georges, *Europhys. Lett.* **84**, 37006 (2008).
 - ³² J. P. Hu and H. Ding, arXiv:1107.1334 (2011).
 - ³³ J. P. Hu, B. Xu, W. Liu, N. Hao, and Y. P. Wang, arXiv:1106.5169 (2011).
 - ³⁴ O. J. Lipscombe, G. F. Chen, C. Fang, T. G. Perring, D. L. Abernathy, A. D. Christianson, T. Egami, N. Wang, J. Hu, and P. Dai, *Phys. Rev. Lett.* **106**, 057004 (2011).
 - ³⁵ M. Wang, C. Fang, D.-X. Yao, G. Tan, L. W. Harriger, Y. Song, T. Netherton, C. Zhang, M. Wang, M. B. Stone, W. Tian, J. Hu, P. Dai, *Nature Communications* **2**, 580 (2011).